

Polyvalent Display of Heme on Hepatitis B Virus Capsid Protein through Coordination to Hexahistidine Tags

Duane E. Prasuhn, Jr.,^{1,2,6} Jane Kuzelka,^{1,2,6} Erica Strable,^{1,2} Andrew K. Udit,^{1,2} So-Hye Cho,^{1,2} Gabriel C. Lander,^{3,4} Joel D. Quispe,^{3,4} James R. Diers,⁵ David F. Bocian,⁵ Clint Potter,^{3,4} Bridget Carragher,^{3,4} and M.G. Finn^{1,2,*}

¹Department of Chemistry

²The Skaggs Institute for Chemical Biology

³Department of Cell Biology

⁴The National Resource for Automated Molecular Spectroscopy

The Scripps Research Institute, La Jolla, CA 92037, USA

⁵Department of Chemistry, University of California, Riverside, Riverside, CA 92521, USA

⁶These authors contributed equally to this work.

*Correspondence: mgfinn@scripps.edu

DOI 10.1016/j.chembiol.2008.03.018

SUMMARY

The addition of a hexahistidine tag to the N terminus of the hepatitis B capsid protein gives rise to a self-assembled particle with 80 sites of high local density of histidine side chains. Iron protoporphyrin IX has been found to bind tightly at each of these sites, making a polyvalent system of well-defined spacing between metalloporphyrin complexes. The spectroscopic and redox properties of the resulting particle are consistent with the presence of 80 site-isolated bis(histidine)-bound heme centers, comprising a polyvalent b-type cytochrome mimic.

INTRODUCTION

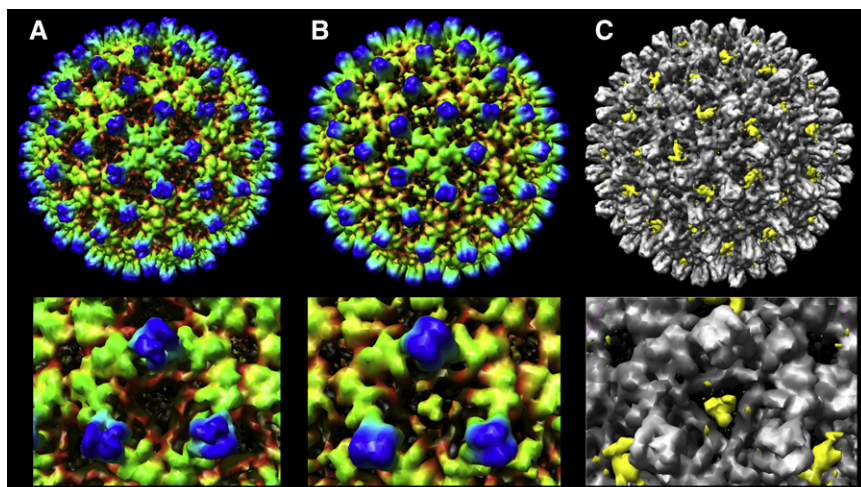
Iron porphyrins (hemes) are among the most versatile cofactors utilized in nature (Chapman et al., 1997). Heme-containing proteins perform crucial biological functions such as substrate oxidation (Ortiz de Montellano, 1995), electron transfer (Gray and Winkler, 1996), and O₂ transport (Antonini and Brunori, 1971). Thus, the design of novel heme systems that either mimic or alter the activity of native metalloproteins is an area of intense interest and active research (Reedy and Gibney, 2004). Site-directed mutagenesis is commonly utilized for direct modification of a protein scaffold (Stayton et al., 1989), whereas the construction of artificial heme protein mimics has been primarily achieved through the synthesis of elaborate small-molecule iron porphyrin compounds (Collman et al., 2004; Feiters et al., 2000) and by the design of heme-binding four-helix bundles (Fahnenschmidt et al., 2001; Reedy et al., 2003; Sakamoto et al., 1999; Shifman et al., 1998). Consequently, numerous structures featuring discrete isolated hemes are available for functional studies. The recent development of scaffolds capable of binding and displaying multiple heme groups is of particular interest (Biemans et al., 1998; Choma et al., 1994; Reedy and Gibney, 2004; Shifman et al., 1998; Weyermann et al., 1999; see also the Supplemental Data available with this article online), inspired by nature's use

of clustered porphyrin-type cofactors for energy collection and multistep electron transfer.

Virus capsids are attractive platforms for the construction of novel nanomaterials including hybrid structures that combine biological macromolecules with inorganic complexes. Numerous reports describe the use of viruses and virus-like particles as platforms for the polyvalent display of materials such as fluorescent dyes and small molecules (Allen et al., 2005; Gillitzer et al., 2002; Hooker et al., 2004; Miller et al., 2007; Schlick et al., 2005; Sen Gupta et al., 2005a; Soto et al., 2006; Wang et al., 2002), electroactive metal complexes (Steinmetz et al., 2006), DNA (Strable et al., 2004), quantum dots (Portney et al., 2005), peptides (Sen Gupta et al., 2005a), carbohydrates (Kaltgrad et al., 2007; Sen Gupta et al., 2005a, 2005b), polymers (Niu et al., 2006; Schlick et al., 2005; Sen Gupta et al., 2005a), and proteins (Sapsford et al., 2006; Sen Gupta et al., 2005a). Our laboratory has recently turned to the core antigen of hepatitis B virus (HBV) as a scaffold for chemical and genetic modification and polyvalent display, following the work of Pumpens and coworkers (Lachmann et al., 1999; Pumpens and Grens, 1999, 2001). We describe here the self-assembly of a polyvalent metalloporphyrin-decorated particle by genetic introduction of potential iron-binding ligands into the capsid structure. Virus scaffolds, and a detailed knowledge of their chemistry, provide the capability to control the density and spacing of light-harvesting units in ways that may prove advantageous in mimicking natural systems. Readers should take note of an elegant report by Francis and coworkers that is particularly relevant to this goal (Miller et al., 2007).

RESULTS AND DISCUSSION

Virus-like particles (VLPs) of HBV are expressed in *Escherichia coli* largely as T = 4 icosahedral particles of ~30 nm diameter, composed of 240 copies of the truncated coat protein (149 amino acids; designated CP149 or wild-type), and displaying 120 four-helix bundles in the form of "spikes" that protrude from the surface of the thin protein shell (Figure 1A; Wynne et al., 1999). Approximately 5% of the particles formed are

**Figure 1. Capsid Structures**

(A and B) Cryoelectron microscopic reconstruction of (A) wild-type HBV (resolution 9.2 Å) and (B) HBV(His₆)₂₄₀ (resolution 8.3 Å).

(C) Difference map, showing in yellow the density observed in HBV(His₆)₂₄₀ but not in wild-type HBV, overlaid on the wild-type HBV density in white. The yellow material therefore presumably represents the His₆ tags inserted at the N terminus of each protein subunit, three of which come together at the three-fold symmetry axis.

Close-up views down a three-fold axis are shown below the whole-particle images.

T = 3 assemblies of 180 capsid proteins, but these can be removed by ultracentrifugation through a 5%–25% sucrose gradient. Genetic modifications of HBV have been made near the tip of the four-helix bundles, as well as at the N and C termini of the protein subunits (Koletzki et al., 1999; Wizemann et al., 2000). We engineered the addition of the sequence His-His-His-His-His-His-Gly-Ala-Ile-Glu-Gly-Asp-Cys to the N terminus, which lies on the outer capsid surface at the edge of the large pore at the three-fold symmetry axis. The construct was expressed in *E. coli* cells, and VLPs were isolated using the protocol described in the **Experimental Procedures**. Here we describe the binding of iron(III) protoporphyrin IX to the modified particles bearing the hexahistidine-containing sequences, designated HBV(His₆)₂₄₀. Whereas the incorporation of His₆ tags into proteins is a common strategy for purification by immobilized metal-affinity chromatography (Gaberc-Porekar and Menart, 2001), we believe this is the first reported example of the use of hexahistidine peptide sequences to anchor transition metal complexes for polyvalent display.

HBV(His₆)₂₄₀ particles were analyzed by cryoelectron microscopy and compared to the particle composed of the wild-type CP149 sequence (Figure 1). The two structures were essentially identical with the exception of additional density occupying a portion of the pore at the three-fold symmetry axis at the base of the protruding four-helix bundles and corresponding to the location of the N terminus. This additional N-terminal density is shown in yellow in Figure 1C, and is similar to a previously reported case of an HBV chimera with an N-terminal peptide extension (Conway et al., 1998). The HBV(His₆)₂₄₀ particles were not retained on an immobilized cobalt column commonly used to bind His-tagged proteins, or on an anion-exchange column (Supplemental Data), in spite of the addition of 1440 histidine residues per particle, indicating that the added sequences were not accessible to the column stationary phase. Presumably, the radial four-helix bundles are not sufficiently flexible to allow a metal-containing surface to interact with His₆ sequences on the “floor” of the capsid structure.

HBV(His₆)₂₄₀ was incubated with one equivalent of iron(III) protoporphyrin IX (Fe[PPIX], or “heme”) per protein subunit in 0.1 M potassium phosphate buffer at pH 7. Purification of the resulting capsids was accomplished by two consecutive sets of sucrose

gradients and ultracentrifugation, resulting in recovery of approximately 40% of the original virions; this yield is somewhat lower than the normal 60%–70% usually obtained with this protocol. Nonspecific adsorption of polyaromatic molecules to virus capsids is common in our experience and two gradients were required for the removal of weakly associated heme, visible as a broad and diffuse band that accompanied the narrow protein band of the purified material. Heme did not associate with HBV particles lacking His₆ tags, or with the individual dimers of disassembled HBV(His₆)₂₄₀ particles, as determined by UV-vis spectroscopy and size-exclusion chromatography (SEC).

Figure 2A shows the SEC analysis of purified heme-HBV(His₆)₂₄₀, confirming their intact nature by coelution of the viral protein (detected at 280 nm) and the heme group (detected at 412 nm) at the volume characteristic of intact particles. Uncomplexed HBV(His₆)₂₄₀ elutes at the same volume, indicating that the modified particles are intact and do not aggregate. The iron(III) centers apparently do not interact significantly with the column resin, consistent with the presence of coordinatively saturated and/or inaccessible metal ions. Heme-HBV(His₆)₂₄₀ was quite stable upon extended storage (several weeks at 4°C), notable because the covalent attachment of polyaromatic dye molecules was found in separate work to cause capsid decomposition, presumably by disruption of noncovalent interactions between subunits.

A loading of 80 ± 8 heme units per particle was established by a combination of quantitative protein assay and inductively coupled plasma optical emission spectrometry (ICP-OES) for iron, for multiple preparations of heme-HBV(His₆)₂₄₀. This value represents the binding of one heme for every three protein subunits, suggesting that the close positioning of the His₆ tags at each three-fold symmetry axis provides a single heme binding pocket. It seems likely that one heme is bound at this location by 2 of the 18 histidine amino acids provided by three adjacent His₆ tags, and there is either no room or insufficient conformational freedom to provide histidine ligands for a second Fe-porphyrin moiety. Cryo-EM analysis of heme-HBV(His₆)₂₄₀ showed no significant difference in structure compared to the particle before treatment with heme (data not shown), suggesting that either the bound heme is found in a range of structurally distinct conformations among the 80 binding sites and so is not visualized upon

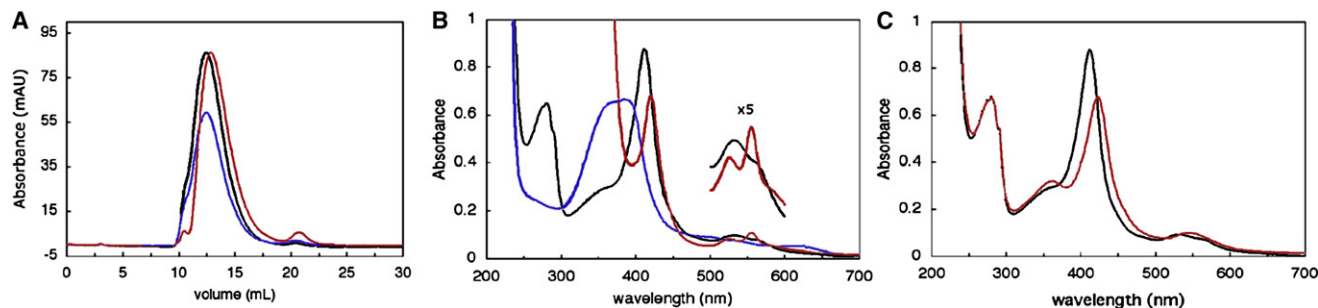


Figure 2. Characterization of Heme-Derivatized HBV Particles

(A) Size-exclusion FPLC of (heme)₈₀HBV(His₆)₂₄₀ showing 280 nm (black) and 412 nm (blue) absorption traces. The trace of HBV(His₆)₂₄₀ (red) is shown for comparison.

(B) UV-vis spectra of oxidized (black) and reduced (red) (heme)₈₀HBV(His₆)₂₄₀ (0.3 mg/ml VLP, 5.6 μM iron) in 0.1 M potassium phosphate buffer (pH 7). The intense absorption below 390 nm of the reduced sample is due to sodium dithionite. The spectrum of free iron(III) protoporphyrin IX (blue) is shown for comparison (20 μM, 2% DMSO).

(C) UV-vis spectra of (heme)₈₀HBV(His₆)₂₄₀ (0.3 mg/ml VLP, 5.6 μM iron) in the absence (black) and presence (red) of 1 M cyanide in 0.1 M potassium phosphate buffer (pH 7).

icosahedral signal averaging (likely given the large number of histidine residues present at each three-fold site) or that the bound heme-protein conformation is not sufficiently different to be resolved at the approximately 9 Å resolution of the reconstruction.

The attachment of Fe(PPIX) to HBV(His₆)₂₄₀ was further confirmed using UV-vis spectroscopy (Figure 2B). In the absence of capsid, Fe(PPIX)Cl in 9:1 buffer:DMSO exhibited a broad Soret band centered at ~375 nm. In contrast, (heme)₈₀HBV(His₆)₂₄₀ is characterized by a narrow Soret band at 412 nm ($\epsilon \approx 156,000 \text{ M}^{-1} \text{ cm}^{-1}$) and Q bands at 533 nm ($\epsilon \approx 18,000 \text{ M}^{-1} \text{ cm}^{-1}$) and 564 nm ($\epsilon \approx 14,000 \text{ M}^{-1} \text{ cm}^{-1}$). Reduction of Fe(III) to Fe(II) by the addition of a small amount of solid sodium dithionite was evidenced by a shift of the Soret band to 420 nm ($\epsilon \approx 120,000 \text{ M}^{-1} \text{ cm}^{-1}$) and the appearance of two distinct and sharp Q bands at 526 and 555 nm ($\epsilon \approx 15,000$ and $20,000 \text{ M}^{-1} \text{ cm}^{-1}$, respectively). These changes were reversible, as removal of the reductant by either dialysis or sucrose gradients regenerated the Fe(III) form. The spectroscopic features exhibited by (heme)₈₀HBV(His₆)₂₄₀ are indicative of low-spin iron(III) porphyrin ligated by two axial imidazole (histidine) groups, as observed for b-type cytochromes (Adar, 1978).

Resonance Raman spectroscopy is highly sensitive to heme axial ligation and supported the assignment of low-spin bis(histidine) axial coordination for (heme)₈₀HBV(His₆)₂₄₀. The high-frequency Soret-excitation resonance Raman spectra of the polyvalent heme particle in 0.1 M potassium phosphate buffer at pH 7 are shown in Figure 3A. The ferric form was characterized by strong bands at ~1640, 1580, 1507, and 1375 cm^{-1} , which shift to ~1626, 1592, 1496, and 1360 cm^{-1} in the ferrous form. These features closely match those of other low-spin bis(histidine)-ligated hemes, and are consistent with minimal structural rearrangement accompanying the reduction to iron(II) (Kalsbeck et al., 1996; Shifman et al., 1998). Importantly, because there is no evident broadening or splitting of the resonance Raman bands, all the capsid-bound hemes can be described as having essentially the same coordination environment (Kalsbeck et al., 1996; Shifman et al., 1998).

The redox potentials of bis(histidine)-ligated heme proteins range from -412 to +360 mV versus the normal hydrogen

electrode (NHE), indicating the significant influence that polypeptides can have on the heme redox potential (Reedy and Gibney, 2004; Tezcan et al., 1998). Cyclic voltammetry (CV) of a degassed solution of (heme)₈₀HBV(His₆)₂₄₀ in 0.1 M potassium phosphate buffer at pH 7 (Figure 3B) revealed a well-defined redox couple with $E_{1/2} = -335$ mV versus Ag/AgCl (-138 mV versus NHE), consistent with the Fe(II)/Fe(III) redox process of HBV-bound, bis(histidine)-ligated heme and comparable to that of hemes coordinated by four-helix bundles (Reedy and Gibney, 2004). For comparison, free heme in solution displayed quasi-reversible redox behavior with a well-defined cathodic peak ($E_{p,c} = -383$ mV) and a broad anodic wave (see the Supplemental Data), whereas the redox potential of free (Fe[protoporphyrin IX][imidazole]₂)⁺ under the same conditions was found to be -420 mV versus Ag/AgCl (-223 V versus NHE), comparable to the previously reported value (Shifman et al., 1998). These observations further support the assignment of the observed redox process in Figure 3B as being due to the HBV(His₆)₂₄₀-bound heme.

The peak current measured for (heme)₈₀HBV(His₆)₂₄₀ was directly proportional to scan rate over a large range (50–750 mV/s), indicating a surface-confined species. Integration of the peaks in Figure 3B yielded a cathodic:anodic charge ratio ($Q_{p,c}:Q_{p,a}$) of 0.93, consistent with chemical reversibility. The amount of adsorbed electroactive heme was estimated, based on the cathodic charge passed, to be approximately 83 hemes/particle (assuming monolayer coverage), in good agreement with the measured loadings. Although the data are consistent with a monolayer of HBV(His₆)₂₄₀ on the electrode surface, the associated heme groups display voltammetric responses atypical of simple surface-confined electrochemistry (Bard and Faulkner, 2001). As suggested in other cases (Clark and Bowden, 1997; Zhang et al., 1997), such deviations likely arise from different redox-active microenvironments produced by adsorption of the polyvalently decorated virus-like particle to the electrode surface. A range of formal potentials and electron transfer rates can be expected to contribute to the observed nonidealities, for example, differential interactions with the electrode surface and varying heme-electrode distances (Tanimura et al., 2002; Tezcan et al., 1998).

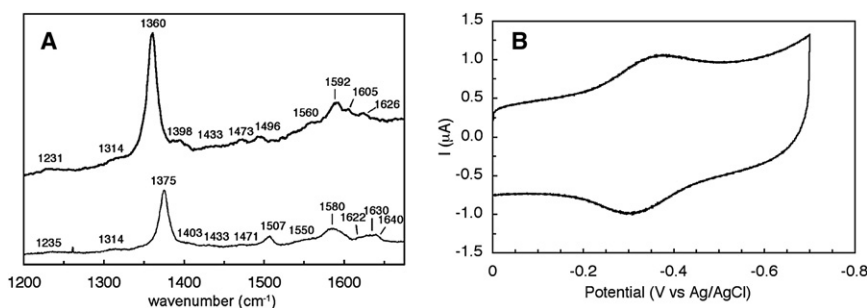


Figure 3. Evidence for Homogeneous Coordination of Heme Units

(A) High-frequency Soret-excitation spectra of (heme)₈₀HBV(His₆)₂₄₀ in the ferric ($\lambda_{\text{ex}} = 406.7$ nm, bottom) and ferrous states ($\lambda_{\text{ex}} = 413.1$ nm, top) in 0.1 M potassium phosphate buffer (pH 7).

(B) Cyclic voltammogram of (heme)₈₀HBV(His₆)₂₄₀ (10 mg/ml, ~ 185 μM iron) in 0.1 M potassium phosphate buffer (pH 7), recorded at 250 mV/s with a glassy carbon working electrode.

The strong nature of the interactions of HBV(His₆)₂₄₀ with Fe(PPIX) was indicated by the addition of competing ligands. No spectral changes were observed when (heme)₈₀HBV(His₆)₂₄₀ was treated with the moderate-field azide ligand (Huang and Kassner, 1979; Rousseau et al., 1989) in up to 1 M concentration ($\sim 10^5$ equivalents azide with respect to Fe). The system was also somewhat resistant to the stronger cyanide ligand. From 0.5–10 mM added KCN (~ 100 –2000 equivalents per Fe), a modest shift of the Soret band from 412 to 415 nm was observed with isosbestic behavior (Supplemental Data). The identity of the species thus formed is not clear. The displacement of either or both coordinated histidine imidazoles would give (Fe[heme][CN])₈₀HBV(His₆)₂₄₀ or (Fe[heme][CN]₂)⁻. The latter species and an analog of the former are both known to show greater shifts in the Soret band (420–425 nm) (de Lauzon et al., 2002; DeVito and Asher, 1989). On the other hand, the addition of as little as 1 mM KCN (~ 100 equivalents with respect to Fe) suppressed the electrochemical response of Figure 3B within the accessible potential window, suggesting some kind of binding to the electroactive iron center. Upon the addition of 100 mM cyanide ($\sim 10^4$ equivalents per Fe), a more pronounced (nonisosbestic) spectroscopic change occurred in the electronic spectrum, with a Soret band at 422 nm ($\epsilon \approx 121,000$ M⁻¹ cm⁻¹) and a single Q band absorption at 545 nm ($\epsilon \approx 18,000$ M⁻¹ cm⁻¹) (Figure 2C), but again no visible electrochemical signal. Control experiments performed in the absence of HBV(His₆)₂₄₀ showed that free Fe(PPIX) was easily detected by cyclic voltammetry under the same conditions both in the presence and absence of KCN, and also in the presence of a large excess of BSA. Furthermore, when we tried to isolate a cyanide-coordinated heme-HBV(His₆)₂₄₀ complex away from excess cyanide by dialysis or sucrose-gradient ultracentrifugation, the putative bound cyanide was lost and the starting (heme)₈₀HBV(His₆)₂₄₀ complex was regenerated. These results suggest that the heme unit is not extracted from the HBV particle by cyanide ion.

SIGNIFICANCE

We show here the selective incorporation of 80 heme moieties onto the surface of HBV via bis(imidazole) coordination of capsid N-terminal His₆ tags, providing a facile route to polyvalent electroactive particles. The binding site is formed by the symmetry of the HBV scaffold, which gives rise to a clustering of three His₆ sequences in a compact space at 80 positions around the 30 nm diameter object. This type

of highly leveraged self-assembly is provided by virus capsid particles more easily than by any other class of proteins, laying the foundation for further construction of nanomaterials with catalytic, electron-transfer, or light-harvesting capabilities.

EXPERIMENTAL PROCEDURES

CP149 HBV Plasmid Construction

A pET-11c plasmid containing the sequence for the first 149 amino acids of the coat protein, designated CP149, was a generous gift from Adam Zlotnick of the Oklahoma University Health Sciences Center. In order to place the capsid protein under inducible control, the *cp149* gene was amplified from the pET-11c plasmid using the following primers, with residues in bold constituting restriction sites used for cloning: *cp149f*: 5'-AAG AAG GAG GAT ATA **GGT CTC AC** ATG GAC ATT GAC CCT-3' and *cp149r*: 5'-TCG GGC TTT GTT AGC AGC CGG **AAG CTT** ATA CTA AAC AAC CGT-3'. The PCR product was sequentially digested with HindIII and BsaI, and then ligated into a pQE-60 plasmid which had been sequentially digested with HindIII and NcoI. (BsaI cleaves one to five bases downstream from its recognition site. The DNA sequences were designed with this in mind, to give compatible ends with NcoI ligation without introducing unwanted sequence into the plasmid.) The resulting plasmid was transformed into competent M15MA cells (a generous gift from David Tirrell at Caltech) harboring the pREP4 plasmid yielding the expression cells M15MA(pQE-60/CP149).

HBV(His₆)₂₄₀ Construction in Vector pQE-60

The His₆-tagged construct consisted of hexahistidine peptide, two spacer amino acids, the Factor Xa cleavage sequence, and a cysteine residue placed before the CP149 sequence. The incorporation of the Factor Xa cleavage site was designed to allow removal of the histidine tag if necessary but was not used. The requisite gene was constructed by amplifying *cp149* using the following primers, with residues in bold constituting restriction sites used for cloning: *his-hbvf*: 5'-AAG AAG GAG GAT ATA **GGT CTC ACC** ATG CAC CAT CAC CAT CAC CAT GCA GGA ATC GAG GG AGAC TGT GAC ATT GAC CCT TAT AAA GAA-3' and *his-hbvr*: 5'-TGC GGC TTT GTT AGC AGC CGG **AAG CTT** ATC CTA AAC AAC CGT-3'. The PCR product was sequentially digested with HindIII and BsaI and ligated into pQE-60 that was previously digested with HindIII and NcoI. The resulting plasmid was transformed into M15MA competent cells yielding the expression cells M15MA(pQE-60/His tag HBV).

HBV(His₆)₂₄₀ Construction in Vector pET-28b

During the course of the study, we experienced some difficulty with expression from the pQE-60 plasmid due to an acquired deletion mutation in the promoter region. While this problem was being diagnosed, expression was transferred to the pET-28b vector, as described below. The resulting particles were identical to those obtained from pQE-60 in M15MA cells, but only a small subset of the work described here was performed with the pET-28b system.

The gene encoding the truncated HBV(His₆)₂₄₀ coat protein was amplified by PCR to incorporate NcoI and HindIII restriction sites at the N-terminal methionine and immediately after the stop codon, respectively. The PCR product and the T7 expression vector pET-28b were separately digested with NcoI and

HindIII, purified by agarose gel electrophoresis, and ligated with T4 DNA ligase. Cloning was performed using Top10 cells, and the final vector sequence was confirmed by standard DNA sequencing. The pET-28b plasmid containing the HBV(His₆)₂₄₀ coat protein gene was transformed into *E. coli* BL21 (DE3 pLysS) cells. Details are below; note that the bacteria were grown in SOB media containing the antibiotics kanamycin and chloramphenicol (50 and 34 µg/ml, respectively), the cells were induced with 1 mM isopropyl-β-D thiogalactosidase (IPTG) and harvested after 3 hr, and lysozyme was omitted from the cell lysis buffer.

Expression and Isolation of CP149 HBV and HBV(His₆)₂₄₀

A single colony of cells expressing either CP149 HBV or HBV(His₆)₂₄₀ was grown overnight in 5 ml of SOB media containing carbenicillin (100 µg/ml) and kanamycin (50 µg/ml). The entire 5 ml starter culture was transferred into 500 ml of fresh SOB media supplemented with carbenicillin (100 µg/ml) and kanamycin (50 µg/ml) and allowed to grow until an OD₆₀₀ of 1.0 was reached. IPTG was added to a final concentration of 1 mM. Induction at 37°C was carried out overnight for approximately 16 hr. Cells were harvested and could be stored at -80°C for months.

A total of 30–60 g of cells was allowed to thaw at room temperature and the cells were resuspended in 50 ml of distilled water. Following resuspension, 200 ml of cold lysis buffer (50 mM HEPES [pH 8.0], 500 mM NaCl, 0.1 mg/ml DNase 1, and 0.1 mg/ml RNase A) was added. The cells were lysed using three cycles of sonication for 2 min, separated by a 2 min rest between cycles. One milligram of lysozyme was then added per ml of lysis buffer and the solution was stirred at 4°C for 1–2 hr. Insoluble cell debris was removed by centrifugation at 10,000 rpm for 30 min. Ammonium sulfate was added to the supernatant to a final concentration of 40% of saturation and allowed to stir at room temperature for 30 min. The precipitated HBV coat protein was separated by centrifuging the sample at 10,000 rpm for 30 min, followed by resuspension of the precipitated protein in 50 ml of buffer. Any insoluble material was removed by centrifugation at 10,000 rpm for 15 min. NaCl was added to a final concentration of 0.5 M and the HBV coat protein was allowed to assemble overnight. Assembled virus-like particles were separated from smaller proteins by ultracentrifugation at 42,000 rpm for 6 hr at 4°C. The pelleted capsid was resuspended in 3–10 ml of buffer and further purification was accomplished by ultracentrifugation through a 10%–40% sucrose gradient for 6 hr at 4°C. Finally, the VLPs were concentrated by repeating the ultracentrifugation step. Separation of the T = 3 and T = 4 particles was accomplished by running no more than 10 mg of capsid on a 5%–30% sucrose gradient at 28,000 rpm for 5 hr.

Characterization of HBV Particles

The purity of the isolated HBV particles was assessed using a variety of biochemical techniques. An A₂₆₀:A₂₈₀ ratio of 0.6–0.7 was typically observed, consistent with the fact that the particles do not encapsidate nucleic acid. The presence and relative amounts of individual, aggregated, and disassembled particles were determined by FPLC, and the purity of the protein particles was established as >95% by SDS-PAGE. Samples were also routinely examined by negative-stain transmission electron microscopy by applying particles at a concentration of 0.2 mg/ml to a carbon-coated formvar transmission electron grid. The grids were stained with 2% uranyl acetate, and visualized by a Phillips CM120 transmission electron microscope. These observations always correlated well with FPLC characterization, in that no evidence of broken particles was observed for routine samples by either technique. Concentrations of unmodified HBV(His₆)₂₄₀ were measured by absorbance at 280 nm; capsids at 1 mg/ml yield an absorbance of 1.74. An overlapping absorption at 280 nm by iron(III) protoporphyrin IX necessitated the use of a Coomassie Plus protein assay (Pierce) for the determination of (heme)₈₀HBV(His₆)₂₄₀ concentrations. A standard curve for the protein assay was constructed using concentrations of 0.1–1 mg/ml of HBV(His₆)₂₄₀.

Anion-Exchange FPLC

The inability of HBV(His₆)₂₄₀ particles to bind to a cobalt column suggested that their effective surface charge might also be changed by the addition of 1440 histidine residues to a smaller degree than anticipated. To explore this question, anion-exchange FPLC was performed, and identical elution profiles were observed for the CP149 and HBV(His₆)₂₄₀ particles (Supplemental Data). We have previously shown that surface charge changes in cowpea mosaic

virus and bacteriophage Qβ of much smaller magnitude are detectable by changes in retention time using this method, and so we conclude that the effective charge of the surface that interacts with the column is unchanged by the addition of the N-terminal histidine tag sequence. Therefore, the surface interactions must be dominated by the four-helix bundles.

Preparation of Samples for Cryoelectron Microscopy

Samples for cryo-EM were cleansed of the 5% of T = 3 virus-like particles by sucrose-gradient ultracentrifugation as described above. Excess sucrose was removed and the samples were concentrated by ultracentrifugation. The pellets were resuspended in buffer to give final concentrations of at least 10 mg/ml.

Cryoelectron Microscopy and Analysis

Samples were prepared for cryo-EM analysis by preservation in vitreous ice via placing 4 µl of sample (~10 mg/ml) and rapid-freeze plunging onto plasma-cleaned Cflat carbon film grids using a Vitrobot (FEI). Data collection was performed by Tecnai F20 electron microscopes (FEI) operating at 120 keV using a dose of ~20e⁻/Å² and a nominal underfocus of 1–4 µm utilizing Legikon data collection software (Suloway et al., 2005). For the reconstructions, 738 micrographs of wild-type HBV and 534 micrographs of HBV(His₆)₂₄₀ were collected at a nominal magnification of 80,000× at a pixel size of 0.14 nm at the specimen. All micrographs were collected on a 4 k × 4 k CCD camera (Gatan).

The contrast transfer function (CTF) for each micrograph was estimated using the automated CTF estimation (ACE) package (Mallick et al., 2005). Wild-type HBV particles (8,906) and HBV(His₆)₂₄₀ (23,187) particles were extracted from the collected data at a box size of 304 × 304 pixels. The HBV particles were binned by a factor of two for the reconstruction. Phase correction of the single particles and subsequent three-dimensional refinement was carried out with the EMAN software package (Ludtke et al., 1999). The amplitudes of the resulting refined structures were adjusted with the SPIDER software package (Frank et al., 1996). Resolution of the final densities was determined to be 9.2 and 8.3 Å, respectively, according to 0.5 Fourier shell correlation criteria. Rigid-body docking of crystal structures into the reconstruction density (not shown) and graphical representations were produced by the Chimera visualization software package (Goddard et al., 2005, 2007).

Preparation of (Heme)₈₀HBV(His₆)₂₄₀

To HBV(His₆)₂₄₀ (40 mg) in buffer (14 ml) was added a DMSO solution of Fe(III) protoporphyrin IX (1 mM, 2.2 ml). The volume of DMSO was increased (1.8 ml) such that the total organic solvent comprised ~20% (v/v) of the total solution. The resulting dark red solution was incubated at room temperature for 1 hr. The reaction mixture was then distributed equally among six 40 ml 10%–40% sucrose gradients and purified by ultracentrifugation at 28,000 rpm for 6 hr. A broad diffuse brown band of lower density than the tight red protein band was discarded. Protein bands were combined and ultracentrifuged at 42,000 rpm for 6 hr, and the resulting red pellets were resuspended in buffer (~2 ml/pellet). Undissolved material was removed by low-speed centrifugation at 9,500 rpm for 15 min. A second set of sucrose gradients, followed by ultracentrifugation, afforded pure (heme)₈₀HBV(His₆)₂₄₀ (15 mg, 38%). Cryo-EM analysis of (heme)₈₀HBV(His₆)₂₄₀ was unable to resolve any differences in structure compared to the HBV(His₆)₂₄₀ starting material.

Resonance Raman Spectroscopy

Resonance Raman spectra were acquired with a Spex 1877 triple spectrograph equipped with a holographically etched 2400 groove/mm grating in the final stage. A camera lens (Canon 50 mm f/1.4) was used to collect the scattered light at 90° to the incident laser beam. The excitation wavelengths of 406.7 and 413.1 nm were provided by the outputs of a Coherent Innova 200-K3 Kr ion laser. An 1152 × 298 pixel, front-illuminated, UV-enhanced, charge-coupled device (CCD) was employed as the detector (Princeton Instruments; LN/CCD equipped with an EEV 1152-UV chip). The laser powers were typically 5 mW, and the frequencies were calibrated using the known frequencies of indene and CCl₄. The accuracy of strong and/or isolated bands is ± 1 cm⁻¹. The slit widths were set to provide ~2 cm⁻¹ resolution.

Electrochemistry

Cyclic voltammograms were recorded using a CH Instruments Electrochemical Workstation. A glassy carbon working electrode (0.07 cm²), an Ag/AgCl

reference electrode, and a platinum wire auxiliary electrode were used. The working electrode was polished with a 0.3 μm alumina slurry, followed by brief sonication. Electrochemical measurements were conducted at ambient temperature under argon in a two-compartment cell separating the reference electrode from the working and counter electrodes with a modified Luggin capillary. Samples of (heme)₅₀HBV(His₆)₂₄₀ were first degassed by ~20 vacuum/argon backfill cycles, then gently purged with argon immediately prior to voltammetry. All other solutions were thoroughly degassed with argon. Estimation of the electrode monolayer coverage was performed as follows. Integration of the area under the peak of Figure 3B yields a value of approximately 100 nC or ~1 pmol heme. A particle of 35 nm diameter has a cross-sectional area of $9.6 \times 10^{-12} \text{ cm}^2/\text{molecule}$. On an electrode with area 0.07 cm^2 , the theoretical monolayer coverage corresponds to 0.012 pmol of HBV.

SUPPLEMENTAL DATA

Supplemental Data include three figures and Supplemental Experimental Procedures and can be found with this article online at <http://www.chembiol.com/cgi/content/full/15/5/513/DC1/>.

ACKNOWLEDGMENTS

This work was funded by The Skaggs Institute for Chemical Biology and the NIH (EB000432, CA112075, and GM36243); A.K.U. was supported by a fellowship from the Canadian Institutes of Health Research. Cryoelectron microscopy was performed at the National Resource for Automated Molecular Microscopy, which is supported by the NIH NCCR P41 program (RR17573). We are grateful to Adam Zlotnick (Oklahoma University Health Sciences Center) for a generous gift of a CP149 construct in a pET-11c plasmid, from which we made our versions of the inducible expression vectors. We also thank Steven Brown for assistance with VLP cloning and expression, and Michael G. Hill of Occidental College for assistance with electrochemical measurements.

Received: December 1, 2007

Revised: March 17, 2008

Accepted: March 18, 2008

Published: May 16, 2008

REFERENCES

- Adar, F. (1978). Electronic absorption spectra of hemes and hemoproteins. In *The Porphyrins*, Volume 3, D. Dolphin, ed. (New York: Academic Press), pp. 167–209.
- Allen, M., Bulte, J.W.M., Liepold, L., Basu, G., Zywicke, H.A., Frank, J.A., Young, M., and Douglas, T. (2005). Paramagnetic viral nanoparticles as potential high-relaxivity magnetic resonance contrast agents. *Magn. Reson. Med.* **54**, 807–812.
- Antonini, E., and Brunori, M., eds. (1971). *Hemoglobin and Myoglobin in Their Reactions with Ligands* (Amsterdam: North-Holland).
- Bard, A.J., and Faulkner, L.R. (2001). *Electrochemical Methods: Fundamentals and Applications*, Second Edition (New York: Wiley).
- Biemans, H.A.M., Rowan, A.E., Verhoeven, A., Vanoppen, P., Latterini, L., Foekema, J., Schenning, A.P.H.J., Meijer, E.W., de Schryver, F.C., and Nolte, R.J.M. (1998). Hexakis porphyrinato benzenes. A new class of porphyrin arrays. *J. Am. Chem. Soc.* **120**, 11054–11060.
- Chapman, S.K., Daff, S., and Munro, A.W. (1997). Heme: the most versatile redox centre in biology? *Struct. Bond.* **88**, 41–70.
- Choma, C.T., Lear, J.D., Nelson, M.J., Dutton, P.L., Robertson, D.E., and DeGrado, W.F. (1994). Design of a heme-binding four-helix bundle. *J. Am. Chem. Soc.* **116**, 856–865.
- Clark, R.A., and Bowden, E.F. (1997). Voltammetric peak broadening for cytochrome *c*/alkanethiolate monolayer structures: dispersion of formal potentials. *Langmuir* **13**, 559–565.
- Collman, J.P., Boulatov, R., Sunderland, C.J., and Fu, L. (2004). Functional analogues of cytochrome *c* oxidase, myoglobin, and hemoglobin. *Chem. Rev.* **104**, 561–588.
- Conway, J.F., Cheng, N., Zlotnick, A., Stahl, S.J., Wingfield, P.T., and Steven, A.C. (1998). Localization of the N terminus of hepatitis B virus capsid protein by peptide-based difference mapping from cryoelectron microscopy. *Proc. Natl. Acad. Sci. USA* **95**, 14622–14627.
- de Lauzon, S., Mansuy, D., and Mahy, J.-P. (2002). Coordination chemistry of iron(III)-porphyrin-antibody complexes. *Eur. J. Biochem.* **269**, 470–480.
- DeVito, V.L., and Asher, S.A. (1989). UV resonance Raman enhancement of vinyl stretching in ferric protoporphyrin IX: conjugation and preservation of the vinyl π to π^* star transition. *J. Am. Chem. Soc.* **111**, 9143–9152.
- Fahnenschmidt, M., Bittl, R., Schlodder, E., Haehnel, W., and Lubitz, W. (2001). Characterization of de novo synthesized four-helix bundle proteins with metalloporphyrin cofactors. *Phys. Chem. Chem. Phys.* **3**, 4082–4090.
- Feiters, M.C., Rowan, A.E., and Nolte, R.J.M. (2000). From simple to supramolecular cytochrome P450 mimics. *Chem. Soc. Rev.* **29**, 375–384.
- Frank, J., Radermacher, M., Penczek, P., Zhu, J., Li, Y., Ladjadj, M., and Leith, A. (1996). SPIDER and WEB: processing and visualization of images in 3D electron microscopy and related fields. *J. Struct. Biol.* **116**, 190–199.
- Gaberc-Porekar, V., and Menart, V. (2001). Perspectives of immobilized-metal affinity chromatography. *J. Biochem. Biophys. Methods* **49**, 335–360.
- Gillitzer, E., Willits, D., Young, M., and Douglas, T. (2002). Chemical modification of a viral cage for multivalent presentation. *Chem. Comm.*, 2390–2391.
- Goddard, T.D., Huang, C.C., and Ferrin, T.E. (2005). Software extensions to UCSF Chimera for interactive visualization of large molecular assemblies. *Structure* **13**, 473–482.
- Goddard, T.D., Huang, C.C., and Ferrin, T.E. (2007). Visualizing density maps with UCSF Chimera. *J. Struct. Biol.* **157**, 281–287.
- Gray, H.B., and Winkler, J.R. (1996). Electron transfer in proteins. *Annu. Rev. Biochem.* **65**, 537–561.
- Hooker, J.M., Kovacs, E.W., and Francis, M.B. (2004). Interior surface modification of bacteriophage MS2. *J. Am. Chem. Soc.* **126**, 3718–3719.
- Huang, Y.-P., and Kassner, R.J. (1979). Temperature-dependent spin-state equilibrium in an azide-ferric heme octapeptide complex. A model system for the spin equilibria of ferric heme proteins. *J. Am. Chem. Soc.* **101**, 5807–5810.
- Kalsbeck, W.A., Robertson, D.E., Pandey, R.K., Smith, K.M., Dutton, P.L., and Bocian, D.F. (1996). Structural and electronic properties of the heme cofactors in a multi-heme synthetic cytochrome. *Biochemistry* **35**, 3429–3438.
- Kaltgrad, E., Sen Gupta, S., Punna, S., Huang, C.-Y., Chang, A., Wong, C.-H., Finn, M.G., and Blixt, O. (2007). Anti-carbohydrate antibodies elicited by polyvalent display on a viral scaffold and characterization using glycan microarrays. *ChemBioChem* **8**, 1455–1462.
- Koletzki, D., Biel, S.S., Meisel, H., Nügel, E., Gelderblom, H.R., Krüger, D.H., and Ulrich, R. (1999). HBV core particles allow the insertion and surface exposure of the entire potentially protective region of Puumala hantavirus nucleocapsid protein. *Biol. Chem.* **380**, 325–333.
- Lachmann, S., Meisel, H., Muselmann, C., Koletzki, D., Gelderblom, H.R., Borisova, G., Krüger, D.H., Pumpens, P., and Ulrich, R. (1999). Characterization of potential insertion sites in the core antigen of hepatitis B virus by the use of a short-sized model epitope. *Intervirology* **42**, 51–56.
- Ludtke, S.J., Baldwin, P.R., and Chiu, W. (1999). EMAN: semiautomated software for high-resolution single-particle reconstructions. *J. Struct. Biol.* **128**, 82–97.
- Mallick, S.P., Carragher, B., Potter, C.S., and Kriegman, D.J. (2005). ACE: automated CTF estimation. *Ultramicroscopy* **104**, 8–29.
- Miller, R.A., Preseley, A.D., and Francis, M.B. (2007). Self-assembling light-harvesting systems from synthetically modified tobacco mosaic virus. *J. Am. Chem. Soc.* **129**, 3104–3109.
- Niu, Z., Bruckman, M., Kotakadi, V.S., He, J., Emrick, T.S., Russell, T.P., Yang, L., and Wang, Q. (2006). Study and characterization of tobacco mosaic virus head-to-tail assembly assisted by aniline polymerization. *Chem. Commun.*, 3019–3021.
- Ortiz de Montellano, P.R., ed. (1995). *Cytochrome P450: Structure, Mechanism, and Biochemistry* (New York: Plenum Press).

- Portney, N.G., Singh, K., Chaudhary, S., Destito, G., Schneemann, A., Manchester, M., and Ozkan, M. (2005). Organic and inorganic nanoparticle hybrids. *Langmuir* 21, 2098–2103.
- Pumpens, P., and Grens, E. (1999). Hepatitis B core particles as a universal display model: a structure-function basis for development. *FEBS Lett.* 442, 1–6.
- Pumpens, P., and Grens, E. (2001). HBV core particles as a carrier for B cell/T cell epitopes. *Intervirology* 44, 98–114.
- Reedy, C.J., and Gibney, B.R. (2004). Heme protein assemblies. *Chem. Rev.* 104, 617–649.
- Reedy, C.J., Kennedy, M.L., and Gibney, B.R. (2003). Thermodynamic characterization of ferric and ferrous haem binding to a designed four- α -helix protein. *Chem. Comm.*, 570–571.
- Rousseau, D.L., Ching, Y., Brunori, M., and Giacometti, G.M. (1989). Axial coordination of ferric *Aplysia* myoglobin. *J. Biol. Chem.* 264, 7878–7881.
- Sakamoto, S., Obataya, I., Ueno, A., and Mihara, H. (1999). Effects of amino acids substitution of hydrophobic residues on haem-binding properties of designed two- α -helix peptides. *J. Chem. Soc. Perkin Trans. 2*, 2059–2069.
- Sapsford, K.E., Soto, C.M., Blum, A.S., Chatterji, A., Lin, T., Johnson, J.E., Ligler, F.S., and Ratna, B.R. (2006). A cowpea mosaic virus nanoscaffold for multiplexed antibody conjugation: application as an immunoassay tracer. *Biosens. Bioelectron.* 21, 1668–1673.
- Schlick, T.L., Ding, Z., Kovacs, E.W., and Francis, M.B. (2005). Dual-surface modification of the tobacco mosaic virus. *J. Am. Chem. Soc.* 127, 3718–3723.
- Sen Gupta, S., Kuzelka, J., Singh, P., Lewis, W.G., Manchester, M., and Finn, M.G. (2005a). Accelerated bioorthogonal conjugation: a practical method for the ligation of diverse functional molecules to a polyvalent virus scaffold. *Bioconjug. Chem.* 16, 1572–1579.
- Sen Gupta, S., Raja, K.S., Kaltgrad, E., Strable, E., and Finn, M.G. (2005b). Virus-glycopolymer conjugates by copper(I) catalysis of atom transfer radical polymerization and azid-alkyne cycloaddition. *Chem. Comm.*, 4315–4317.
- Shifman, J.M., Moser, C.C., Kalsbeck, W.A., Bocian, D.F., and Dutton, P.L. (1998). Functionalized de novo designed proteins: mechanism of proton coupling to oxidation/reduction in heme protein maquettes. *Biochemistry* 37, 16815–16827.
- Soto, C.M., Blum, A.S., Vora, G.J., Lebedev, N., Meador, C.E., Won, A.P., Chatterji, A., Johnson, J.E., and Ratna, B.R. (2006). Fluorescent signal amplification of carbocyanine dyes using engineered viral nanoparticles. *J. Am. Chem. Soc.* 128, 5184–5189.
- Stayton, P.S., Atkins, W.M., Springer, B.A., and Sligar, S.G. (1989). Site-directed mutagenesis of heme proteins. *Met. Ions Biol. Syst.* 25, 417–475.
- Steinmetz, N.F., Lomonosoff, G.P., and Evans, D.J. (2006). Decoration of cowpea mosaic virus with multiple, redox-active, organometallic complexes. *Small* 2, 530–533.
- Strable, E., Johnson, J.E., and Finn, M.G. (2004). Natural nanochemical building blocks: icosahedral virus particles organized by attached oligonucleotides. *Nano Lett.* 4, 1385–1389.
- Suloway, C., Pulokas, J., Fellmann, D., Cheng, A., Guerra, F., Quispe, J., Stagg, S., Potter, C.S., and Carragher, B. (2005). Automated molecular microscopy: the new Legimon system. *J. Struct. Biol.* 151, 41–60.
- Tanimura, R., Hill, M.G., Margoliash, E., Niki, K., Ohno, H., and Gray, H.B. (2002). Active carboxylic acid-terminated alkanethiol self-assembled monolayers on gold bead electrodes for immobilization of cytochromes c. *Electrochem. Solid-State Lett.* 5, E67–E70.
- Tezcan, F.A., Winkler, J.R., and Gray, H.B. (1998). Effects of ligation and folding on reduction potentials of heme proteins. *J. Am. Chem. Soc.* 120, 13383–13388.
- Wang, Q., Lin, T., Tang, L., Johnson, J.E., and Finn, M.G. (2002). Icosahedral virus particles as addressable nanoscale building blocks. *Angew. Chem. Int. Ed. Engl.* 41, 459–462.
- Weyermann, P., Gisselbrecht, J.-P., Boudon, C., Diederich, F., and Gross, M. (1999). Dendritic iron porphyrins with tethered axial ligands: new model compounds for cytochromes. *Angew. Chem. Int. Ed. Engl.* 38, 3215–3219.
- Wizemann, H., Weiland, F., Pfaff, E., and von Brunn, A. (2000). Polyhistidine-tagged hepatitis B core particles as carriers of HIV-1/gp120 epitopes of different HIV-1 subtypes. *Biol. Chem.* 381, 231–243.
- Wynne, S.A., Crowther, R.A., and Leslie, A.G.W. (1999). The crystal structure of the human hepatitis B virus capsid. *Mol. Cell* 3, 771–780.
- Zhang, Z., Nasar, A.-E., Lu, Z., Schenkman, J.B., and Rusling, J.F. (1997). Direct electron injection from electrodes to cytochrome P450(cam) in biomembrane-like films. *J. Chem. Soc. Faraday Trans.* 93, 1769–1774.